ChemElectroChem

Research Article
doi.org/10.1002/celc.202400450

SAND2024-13323J

Chemistry Europe
European Chemical Societies Publishing

www.chemelectrochem.org

Influence of Linker Group on Bipolar Redox-Active Molecule Performance in Non-Aqueous Redox Flow Batteries

Samantha Macchi,*[a] Chad L. Staiger,[b] Jesse Cordova,[a] Cassandria Poirier,[c] and Travis M. Anderson[a]

Redox flow batteries (RFBs) are an attractive choice for stationary energy storage of renewables such as solar and wind. Non-aqueous redox flow batteries (NARFBs) have garnered broad interest due to their high voltage operation compared to their aqueous counterparts. Further, the utilization of bipolar redox-active molecules (BRMs) is a practical way to alleviate crossover faced by asymmetric RFBs. In this work, ferrocene (Fc) and phthalimide (PI) are covalently linked with various tethering groups which vary in structure and length. The compiled results suggest that the length and steric shielding ability of the linker group can greatly influence the stability and overall performance of Fc-*n*-PI BRM-based NARFBs. Primary sources of capacity loss are found to be BRM degradation for straight chain spacers <6 carbons and membrane (Nafion) fouling. Fc-hexyl-PI provided the most stable battery cycling and coulombic efficiencies of $>98\,\%$ over 100 cycles (~13 days). NARFB using Fc-hexyl-PI as an active material exhibited high working voltage (1.93 V) and maximum capacity (1.28 $Ah\,L^{-1}$). Additionally, this work highlights rational strategies to improve cycling stability and optimize NARFB performance.

1. Introduction

Economic and population growth continues to rapidly drive worldwide energy consumption. Likewise, renewable energy production (solar, wind, etc.) is increasingly popular due to efforts in phasing out fossil fuel usage due to environmental concerns.[1,2] A key issue associated with renewable energy sources is their unpredictable and inconsistent energy generation, causing disruptions to grid stability.[2] Thus, there is a growing need for the development of energy storage systems (ESSs) which can store large amounts of energy and level out irregular energy production. Redox flow batteries (RFBs) offer many advantages over other technologies in this arena such as long lifetimes and superior scalability owing to their decoupled power and energy output.[3,4] These qualities make RFBs incredibly versatile as stationary ESSs. RFBs operate via flowing redox-active species from reservoir tanks onto current-collecting electrodes with a membrane or separator between the two electrodes.[5,6] The cathodic or positive tank is called the posolyte while the anodic or negative tank is referred to as the negolyte.

Commercialized RFB designs are based on aqueous vanadium or other metal-based redox couples.[7] Non-aqueous RFB (NARFB) designs have seen recent growth in popularity due to a significant advantage over water-based cells: their operating voltage windows are not limited by water decomposition.[8,9] Additionally, at laboratory scale, non-aqueous systems can offer a more simplistic analysis approach due to the limited acid/base effects in organic solvents compared to water. However, there are drawbacks to non-aqueous cells that have hindered their commercialization such as higher solvent cost, membrane compatibility issues,[10] and solubility/conductivity limitations.[11] Thus, significant efforts have focused on lowering costs and improving the performance of redox-active molecules in NARFBs. This has included strategies such as improving the solubility and redox potential of organic active materials[12] and use of machine learning methods to streamline materials discovery.[13]

NARFBs based on small molecule active materials traditionally adopt an asymmetric design where the negative and positive charge-storing species differ from each other. This allows for accurate voltage tuning but is highly susceptible to the issues associated with crossover (unwanted migration of active species across a separator), such as low coulombic efficiencies and irreversible capacity losses.[14] One strategy to effectively mitigate the effects of crossover is to utilize a molecularly symmetric cell with bipolar redox-active molecules (BRMs), which operate similarly to the commercial all-vanadium design.[15] This also allows for post-cycling restoration of capacity via cell 'rebalancing' or mixing of reservoir solutions.[16] BRMs contain both the positive and negative half reaction

[a] S. Macchi, J. Cordova, T. M. Anderson
Power Sources R&D, Sandia National Laboratories,
Albuquerque, NM 87123 USA
E-mail: spmacch@sandia.gov

[b] C. L. Staiger
Department of Photovoltaics & Materials Technologies, Sandia National Laboratories, Albuquerque, NM 87123 USA

[c] C. Poirier
Radiation Effects Experimentation, Sandia National Laboratories,
Albuquerque, NM 87123 USA

Supporting information for this article is available on the WWW under https://doi.org/10.1002/celc.202400450

species in a single molecule, typically attached covalently by some linker group. It has recently been demonstrated that the linker group plays a crucial role in the electrochemical properties and performance of BRMs.[17] To maintain stability over continuous cycling, the BRM moieties must be adequately distanced from one another.[17,18] This is especially true for molecules that produce radicals upon charging and exhibit donor-acceptor (D–A) intramolecular charge transfer (ICT), which can destabilize radical species. Other properties of the spacer group (polarity and rigidity) also play a role in the overall cell performance by changing the molecular kinetics and diffusion characteristics. Thus, a study of various linkers could highlight the most efficient pathway to develop highly stable and energy-dense RFBs comprised of BRMs.

In this work, ferrocene (Fc) and phthalimide (PI) were chosen as a redox couple due to their excellent electrochemical properties and ~2 V electrochemical separation. *N*-Ferrocenylphthalimide (Fc-PI) has been previously studied in a coin cell with promising results.[16] However, the cell was cycled at very low current densities (up to 60 $\mu A\,cm^{-2}$) and these results do not guarantee optimal performance in flow battery conditions. Herein, this work aims to study Fc-PI in a laboratory-scale flowing cell design as well as elucidate the effects of the linker group on the flow cell performance of Fc-*n*-PI derivatives. This is achieved through introduction of spacer groups of various length and structure, including: direct linkage, methyl, α-ethyl, butyl, ether, and hexyl moieties. The spacer groups were logically designed based on: 1) increasing chain length of unsubstituted alkyl groups to determine the optimum separation between Fc and PI to reduce ICT, 2) substitution at the α-carbon position to introduce steric shielding and asymmetry, in an effort to reduce π - π stacking and increase solubility, and 3) solvent matching with an ether functional group to improve stability and solubility.

2. Results and Discussion

2.1. Electrochemical Characterization of BRMs

A series of Fc-*n*-PI derivatives were designed and synthesized with various linker groups to study their effect on flow battery performance. First, cyclic voltammograms (CVs) were recorded for each sample to determine their working potential. Fc-PI exhibited an oxidation peak at 0.078 V (vs Fc/Fc^+) and reduction peak at −1.84 V (vs Fc/Fc^+), resulting in a potential difference (ΔE_0) of 1.92 V (Figure 1A). Voltammograms of other samples can be found in the Supporting Information document. One prominent advantage of NARFBs is additionally highlighted in Figure 1A: the 5 V potential window of the non-aqueous supporting electrolyte of 1 M tetrabutylammonium tetrafluoroborate ($TBABF_4$) in 1,3-dioxolane (DOL). The proposed charging and discharging redox mechanisms of Fc-PI are displayed in Figure 1B and the structures, calculated ΔE_0 values, and recorded solubilities of the studied BRMs are given in Figure 1C. Recorded ΔE_0 values range from 1.91–2.07 V amongst BRM derivatives. Values of ΔE_0 decrease with increasing chain length of the spacer (Table S1), excluding Fc-PI. For BRMs with alkyl spacer groups, this phenomenon can be rationalized by stronger ICT interactions when Fc and PI are closer in proximity. Solubilities were determined in 1 M $TBABF_4$ electrolyte solution in DOL via the shake-flask method (Experimental section).

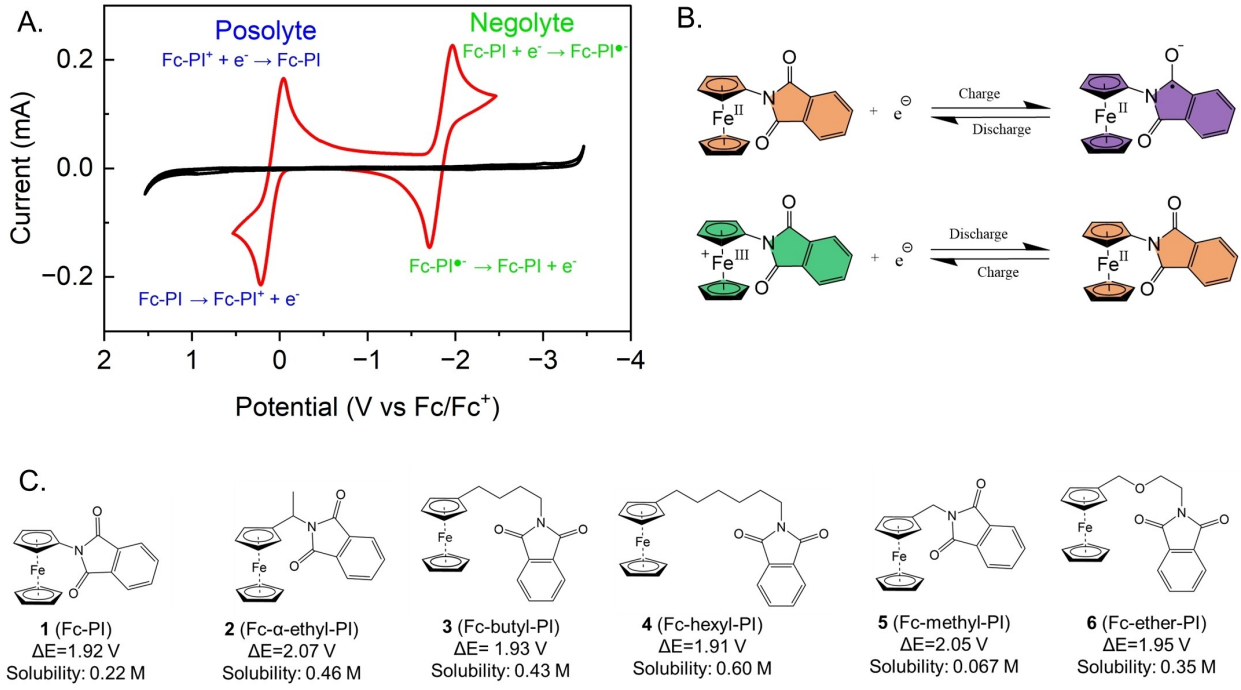

Figure 1. A) Cyclic voltammogram of Fc-PI (red) and supporting electrolyte (1 M $TBABF_4$/DOL) potential window (black) at 100 $mV\,s^{-1}$ scan rate, B) charging mechanism of negolyte and posolyte of Fc-PI cell, and C) library of Fc-n-PI derivatives with various spacer groups, their corresponding measured cell potentials, and solubilities, estimated from shake-flask method.

Directly linked Fc-PI showed moderate solubility of 220 mM and solubility increased when linkers were incorporated (excluding Fc-methyl-PI). The greatest solubility was achieved via the longest (hexyl) spacer group likely due to reduced molecular packing as a result of increased steric repulsion.

Diffusion parameters of Fc-PI were studied by recording voltammograms at various scan rates from 10–250 mV s^{-1} (Figure 2A). A plot of anodic and cathodic current versus the square root of the scan rate (Figure 2B) enabled direct calculation of the diffusion constant, *D*, from the Randles–Ševčík equation (Equation 1 in experimental section). These plots are found for other BRM derivatives in the supporting information document. An average value of 0.15×10^{-6} $cm^2 s^{-1}$ was obtained for Fc-PI (Table S1). All molecules with substituted linkers exhibited *D* values an order of magnitude larger compared to Fc-PI. Among straight-chain linkers, *D* increases slightly from one to four carbon lengths and decreases slightly from four to six carbon lengths (Figure S6). However, there is no significant loss of mobility when increasing the linker up to six carbons in length and this behavior has been seen for other BRMs.[17] Additionally, the rate constant, k^0, was calculated using the Nicholson method (Equation 2 in experimental section) for each BRM (Table S1). Values on the order of 10^{-4} cm s^{-1} were observed for all Fc-n-PI molecules, apart from Fc-PI, which further highlights the necessity for a linking group between redox moieties. Values obtained for the other five BRMs are similar to those reported for non-aqueous active materials.

To uncover the effect of linker (straight) chain length on the kinetic balance of BRM ions, the ratios of cathodic and anodic diffusion constants were compared among BRMs (Figure S6). A ratio that varies from unity is indicative of imbalance in charge diffusion within the cell. Compared to asymmetric molecules,

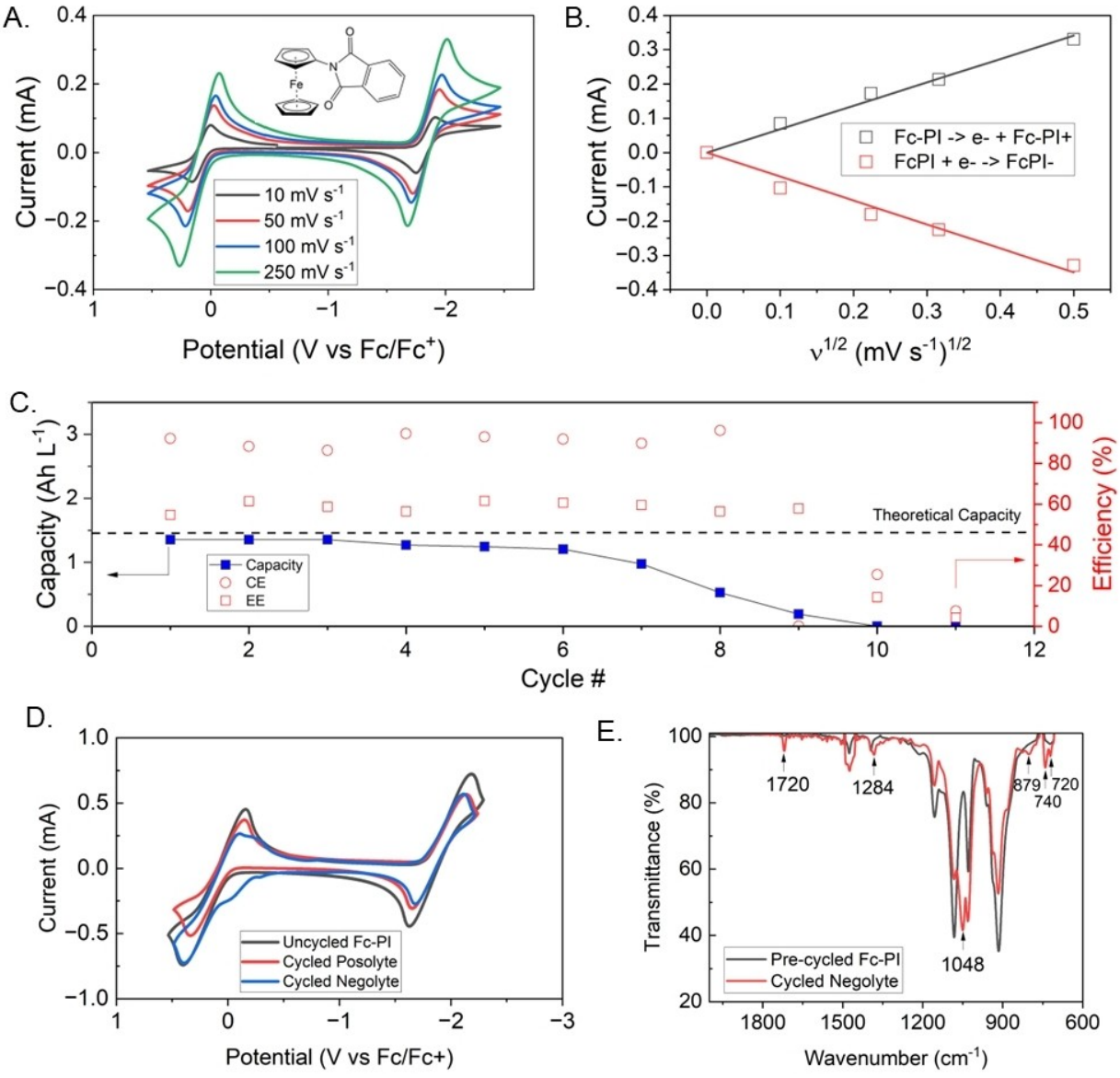

Figure 2. A) CV of Fc-PI at various scan rates, B) plot of anodic and cathodic peak current versus the square root of the scan rate ($v^{1/2}$), C) flow battery cycling of Fc-PI for 11 cycles (until failure), D) CV of posolyte and negolyte post-mortem, and E) FT-IR spectra of Fc-PI pre-cycled and negolyte post-cycling.

BRMs should possess a much more balanced diffusion profile due to the covalent linkage of cathodic and anodic species. All Fc-*n*-PI BRMs exhibited values close to 1, except Fc-PI which showed a ratio of 1.23.

2.2. Flow Battery Performance of BRMs

Fc-PI BRM was previously reported to show excellent performance in a coin cell at very low current loading (up to 60 $\mu A\,cm^{-2}$).[16] In this work, we aimed to uncover the applicability of this molecule under elevated current conditions in a laboratory-scale flow cell. The Fc-PI flow cell was galvanostatically cycled between voltage limits of 2.4 and 1.4 V. These voltages correspond to an effective battery voltage of ~1.9 ± 0.5 V. Fc-PI was cycled ten times before the cutoff potential was rapidly reached, leading to ~100% capacity loss (Figure 2C). Post-mortem CV of negolyte and posolyte revealed the appearance of new oxidation and reduction peaks (Figure 2D) in the negolyte, indicative of molecular degradation of Fc-PI during cycling. It is hypothesized that the degradation of Fc-PI was primarily due to radical reaction of oxygen from PI, as seen in other works.[19,20] Interestingly, the additional peaks were located near the Fc redox couple, indicating an intermolecular attack of Fc by the PI radical in the charged state. CV was additionally recorded after the first and tenth charge cycles (Figure S7) to gauge the relative rate of decomposition. The additional redox peaks appeared in the voltammogram even after one charge, further supporting that Fc-PI degradation was responsible for rapid capacity losses. Fourier transform infrared (FT-IR) spectra (Figure 2E) of the post-cycled negolyte confirmed evidence of molecule degradation, with additional peaks post-mortem. Peaks at 720, 740, and 1284 cm^{-1} are attributed to degradation products generated during radical interaction with supporting electrolyte, solvent, and membrane. Two peaks located at 879 and 1050 cm^{-1} were attributed to the polymerization of DOL solvent; polymerization of DOL is facilitated by unsubstituted protons on Nafion side chains and is expected in a small and constant amount for all cells.[21] Additionally, the post-cycled Nafion membrane developed a brownish fouling over the course of cycling (Figure S8) which was likely responsible for some capacity loss. From these results, it can be concluded that Fc-PI is unsuitable for flow battery application, although at milder conditions, showed promising performance.[22]

Huang and coworkers[23] found that the introduction of an α-ethyl linker group to Fc-PI increased its solubility and coin cell cycling stability. However, like Fc-PI, this was investigated at very low current (120 $\mu A\,cm^{-2}$) in a static cell. Like Fc-PI, Fc-α-ethyl-PI was synthesized from commercially available starting materials in a single step (Figure 3A). Flow cell cycling of Fc-α-ethyl-PI was performed over 100 total cycles. To accentuate the bipolar nature of the BRMs, the cell was rebalanced by mixing the negolyte and posolyte reservoirs after 50 cycles. Small increases in the capacity plots were observed which are due to slight temperature fluctuations in the glovebox during cycling and similar effects have been seen previously.[24] A maximum electrochemical yield (ECY) of 95.7% was achieved by the cell during the first cycle. ECY is the percentage of capacity achieved compared to theoretical. Average coulombic efficiency (CE) values of 98.2% indicated little effect of crossover, due to the bipolar nature of the molecule. Energy efficiency (EE) obtained over 100 cycles was 63%, and a 63.7% loss in capacity was observed for Fc-α-ethyl-PI from cycle 1 to cycle 50. After rebalancing, Fc-α-ethyl-PI achieved an ECY of 59.7%, indicating that some of the initial capacity was able to be restored. Post-cycling CV revealed no additional peaks, thus active material degradation was not likely a major driver of capacity loss in the system. However, the overpotential of the cell increased dramatically (~220 mV) from cycle 2 to 45 (Figure 3D), limiting accessible capacity. The increased polarization was attributed to an increased cell resistance identified by electrochemical impedance spectroscopy (EIS) before and after cycling (Figures 3E and F). This was likely due to several reasons: solvent evaporation, membrane fouling, and/or other parasitic side reactions. DOL is a low boiling point solvent and has been found to exhibit a small amount of evaporation even in inert glovebox conditions.[25] A small amount of solvent evaporation over the long cycling time (6.6 days for first 50 cycles) likely increased solution viscosity, causing increased cell resistance and overvoltage. Membrane fouling was also visibly observed, similar to the previous Fc-PI cell. When comparing the FT-IR spectra (Figure S9) of fouled versus pristine membranes, a relative decrease in peaks intensity was noted at ~1090 and ~960 cm^{-1}, corresponding to CF_2 and C–O–C stretches of Nafion side chains.[26] Fouling can alter the ion transport channel structures of Nafion allowing absorption of active material.[27] FT-IR peaks found at 920, 940, 1034, and 1262 cm^{-1} were attributed to active material uptake by Nafion. Capacity loss was also, in part, due to potential incompatibility of the PI radical with other cell components such as the electrolyte anion (BF_4^-).[28] In order to minimize capacity losses, it is imperative to maximize the radical stability of Fc-*n*-PI derivatives.

Despite the non-ideal performance of Fc-α-ethyl-PI, cycling stability was greatly improved compared to Fc-PI (no linker). In order to better understand this enhanced stability, a non-sterically shielded short-chain analog was synthesized, Fc-methyl-PI. Synthesis and NMR details can be found in the supporting information document. Notably, the solubility of Fc-methyl-PI was lower than other analogs (67 mM). This was likely due to more effective molecular packing compared to the sterically bulky Fc-α-ethyl-PI derivative. Flow cell cycling revealed similar results for Fc-methyl-PI and Fc-PI where consistent degradation occurred for the first six cycles, after which there was a rapid decrease in capacity (Figure S10). The enhanced stability of Fc-α-ethyl-PI compared to Fc-methyl-PI illustrates the capability to enhance the radical stability of even short alkane linker groups via introduction of steric shielding.

In an attempt to further improve radical and cycling stability, the linker group was further increased to four carbon lengths (Fc-butyl-PI). It has been previously reported that preventing ICT by physical separation of the posolyte/negolyte moieties can enhance radical stability.[27] Surprisingly, flow cell cycling of Fc-butyl-BRM over 50 cycles (Figure 4A) showed a

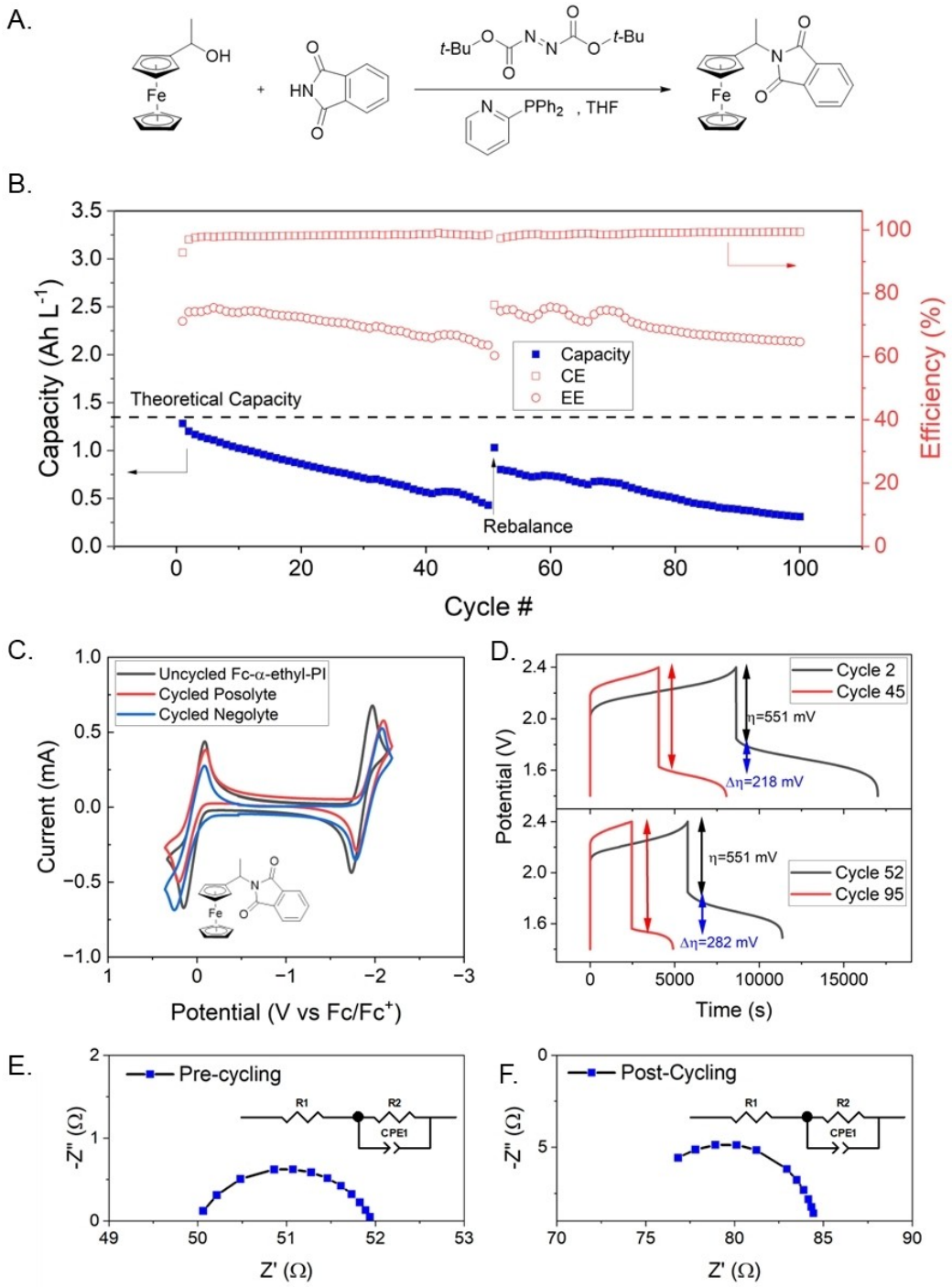

Figure 3. A) synthetic scheme of Fc-α-ethyl-PI, B) flow cell cycling of Fc-a-ethyl-PI for 100 cycles with physical rebalance after 50 cycles, C) post cycling CV, and D) charge-discharge curves of selected cycles near the beginning and end of the first and second 50 cycles, EIS of flow cell E) before cycling and F) after cycling with equivalent circuits shown in inset.

rapid decrease in capacity and after 50 cycles, only 14% of the original capacity was retained. CV of post-cycled Fc-butyl-PI (Figure 4B) shows a decrease in the redox current peaks of PI in the negolyte, but no additional peaks. This result lends toward degradation of PI in the negolyte into redox-inactive by-products. This illustrates the linker groups' influence on the degradation pathway of BRM species. Charge-discharge curves (Figure 4C) show a rise in overpotential over cycling, similar to previous cells. Due to the poor performance of Fc-butyl-BRM, rebalancing was not performed.

To investigate whether the introduction of other functional groups could enhance solubility or radical stability, a methyl-ethyl ether linked analog (Fc-ether-PI) was synthesized and cycled in a flowing cell (Figure S11A). Interestingly, Fc-ether-PI

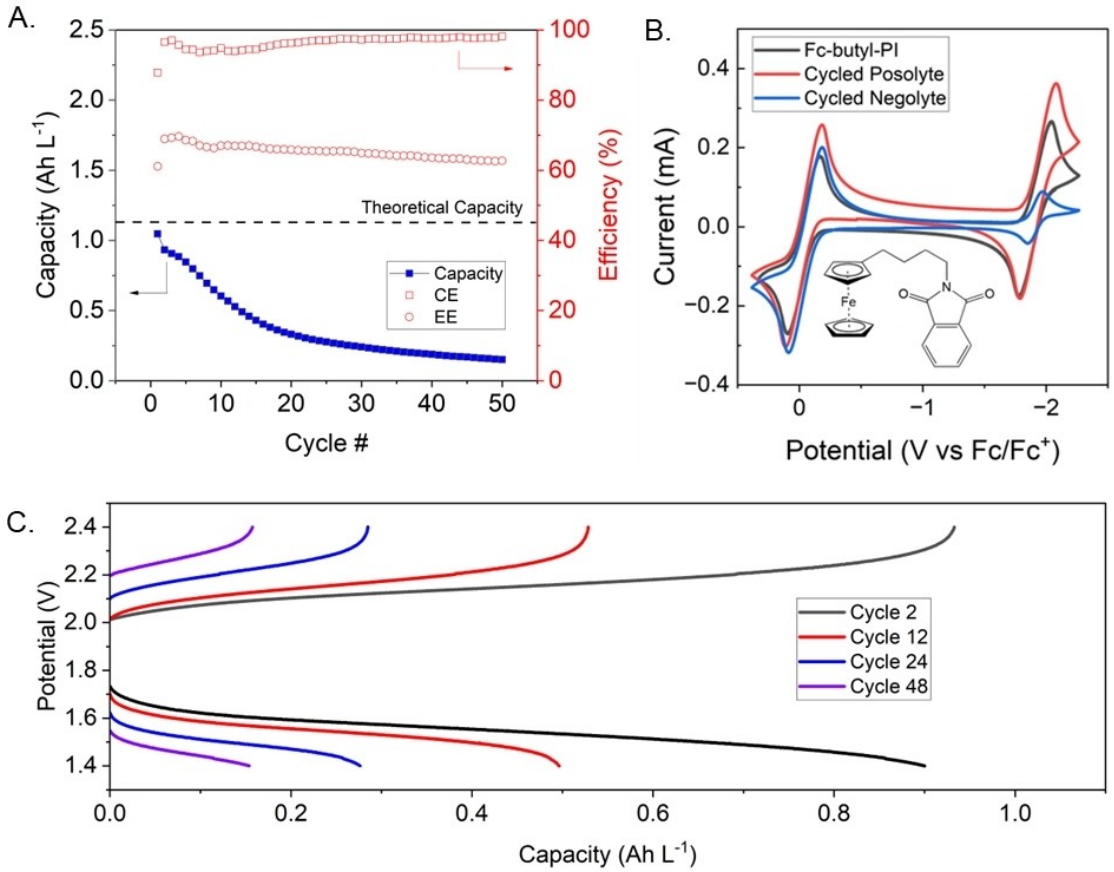

Figure 4. A) flow cell cycling of Fc-butyl-PI for 50 cycles, B) post cycling CV, and C) charge-discharge curves of Fc-butyl-PI at representative cycles.

did not show any enhanced performance compared to Fc-butyl-PI and exhibited a similar post-cycled CV (Figure S11B), indicative of a similar molecular degradation pathway. This result indicates that the ether functional group is incapable of providing any additional stability to the molecule.

Due to the instability of Fc-butyl-PI during cell cycling, a BRM with a hexyl alkane spacer was designed to further separate Fc and PI and further reduce the chance of ICT. Fc-hexyl-PI was cycled for 100 total cycles and rebalanced after cycle 50 (Figure 5A). The cell experienced 47% and 44% capacity loss from cycle 1 to 50 and 51 to 100, respectively. This is greatly improved from the capacity losses of Fc-α-ethyl-PI, which exhibited 64 and 70% capacity loss, respectively. Additionally, 88% of capacity was retained after rebalancing, compared to 59% retention by Fc-α-ethyl-PI. CV of post-cycled active electrolytes showed no additional or loss of peaks (Figure 5B). These results indicate that the increased linker size sufficiently enhanced the PI radical stability, lowering capacity losses. Additionally, charge polarization does not exceed 2.1 V over 100 cycles (Figure 5C), indicating less change in cell resistivity over cycling compared to previous cells. The linker was not further lengthened due to the possibility of intermolecular head-to-toe charge transfer of chain-crossed BRMs that can diminish stability.[27]

It was hypothesized that the improved performance of Fc-hexyl-PI is in part due to lowered membranal diffusion of the larger, more hydrophobic BRM molecule. An experiment was designed in which the negolyte reservoir was filled with 50 mM BRM (Fc-PI or Fc-hexyl-PI) and supporting electrolyte (1 M $TBABF_4$ in DOL) and the posolyte tank was supporting electrolyte only. The electrolytes were pumped for 6.5 h at 20 mL min^{-1}. Afterwards the posolyte was removed and investigated via UV-Visible spectrophotometry (Figure S12). Concentrations of Fc-PI and Fc-hexyl-PI that migrated across the membrane were 1.04 and 0.59 mM, respectively. Thus proving that smaller BRMs were able to much more easily diffuse through the Nafion membrane, leading to greater capacity loss during cycling.

To evaluate the effect of current density on BRM performance, a flow cell containing Fc-hexyl-PI was studied at 1, 1.5, and 2 mA cm^{-2} for ten cycles (Figure 5D). Better capacity retention was obtained with increased current density, which is expected due to faster charge cycles, limiting the lifetime of the active radical species. However, lower capacities were observed due to increased polarization losses at high current densities. Higher current loadings could not be realized for this system due to conductivity limitations of the electrolyte system and Nafion membrane (Figure 3E). Additionally, elevated concentrations (> 0.2 M) of Fc-hexyl-BRM could not be utilized likely due to extreme membrane fouling resulting in rapid (3 cycles) failure of the battery (Figure S13). Advancement in BRM battery

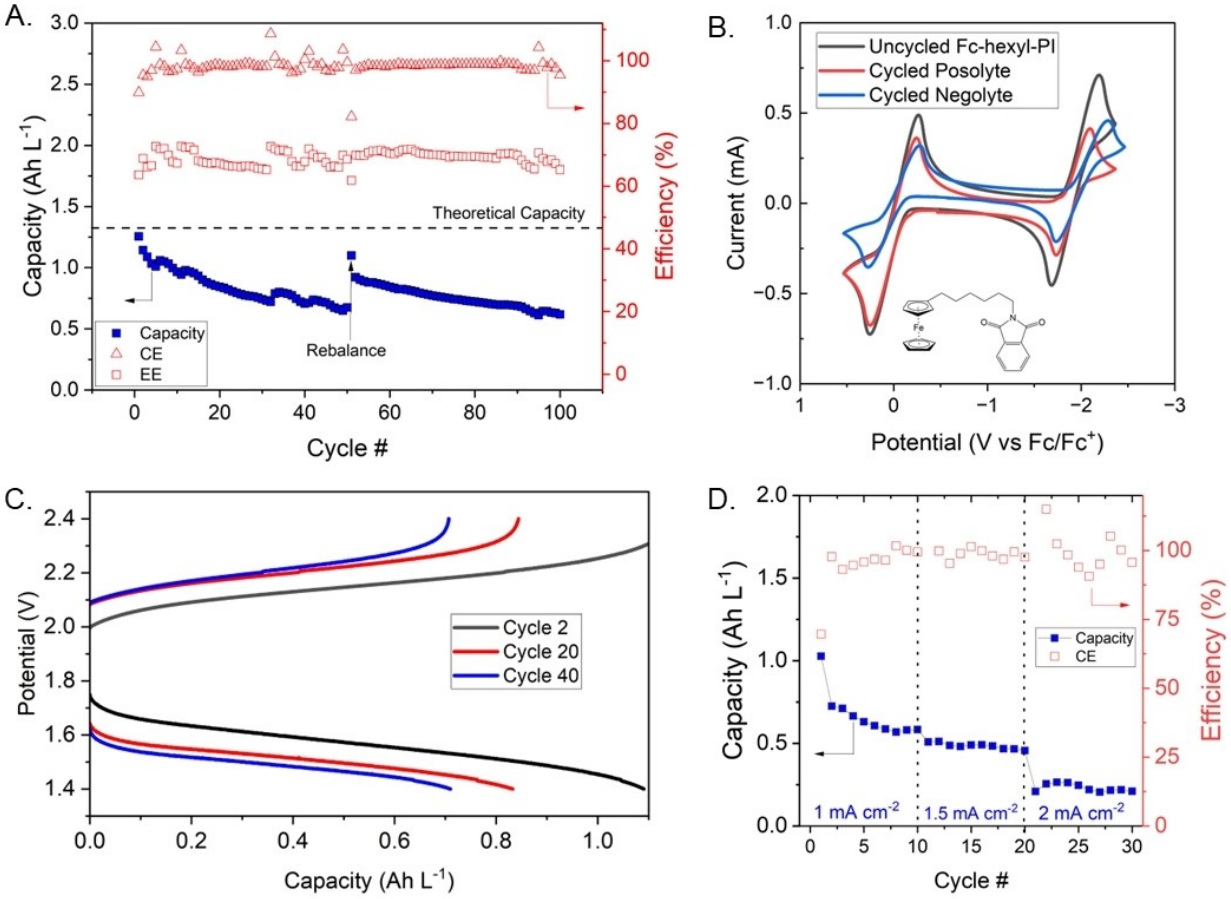

Figure 5. A) flow cell cycling of Fc-hexyl-PI over 100 cycles, B) CV of electrolyte solutions before and after cycling, D) charge-discharge curves, and D) rate capability testing of Fc-hexyl-PI.

performance will require methods to increase both membrane and radical stability.

While Fc-hexyl-PI RFB performance proved that strategic molecular design of BRM linkers can effectively minimize capacity fade, we aimed to further enhance the stability of this molecule by optimizing the supporting electrolyte. Three different solvents: acetonitrile (MeCN), DOL, and 1,2-dimethoxyethane (DME) and three supporting salts: tetrabutylammonium hexafluorophosphate ($TBAPF_6$), tetrabutylammonium bis(trifluoromethanesulfonyl)imide (TBATFSI), and $TBABF_4$ were investigated as potential supporting electrolyte combinations. All salt concentrations utilized were set at 1 M. TBATFSI/DME supporting electrolyte had previously shown to improve flow cell stability, especially towards negolyte radicals.[28] However, for Fc-hexyl-PI active specie, this combination showed the worst capacity retention (Figure 6A) and exhibited extreme membrane fouling after only ten cycles. The $TBAPF_6$/DOL cell exhibited the greatest cycling stability, showing a five percent improvement in capacity retention compared to the original $TBABF_4$/DOL supporting electrolyte after 40 cycles. These results emphasize the importance of optimizing the solvent/salt system for each unique redox couple and further highlights the need to develop more compatible membranes for NARFBs.

Figure 6B highlights the comparison between capacity retention of the four BRMs over 50 cycles (aside from 10 cycles of Fc-PI) as a function of time. It is clear there are length and structure requirements for the linker between Fc and PI in order to obtain sufficient stability to improve capacity retention. For Fc-*n*-PI BRMs, if the linker is a straight chain alkyl group, it must be longer than four carbons in length to achieve reasonable stability. However, methyl substitution at the alpha-carbon can allow for a relatively short linker (methyl) to cycle much more stable than a straight chain linkage of four carbons long. It is worth noting that it is difficult to decouple all of the sources of capacity loss in the studied systems due to the many possible contributors (solvent/membrane interaction, degradation of BRM/supporting salts, membrane fouling, etc.) Among the synthesized BRMs, Fc-hexyl-PI displayed extraordinary maximum capacity and cell voltage compared to recently studied BRMs (Table 1). For other works using ion exchange membranes, the current densities used in this study are comparable to previous studies, with greater working voltages and capacity utilization.

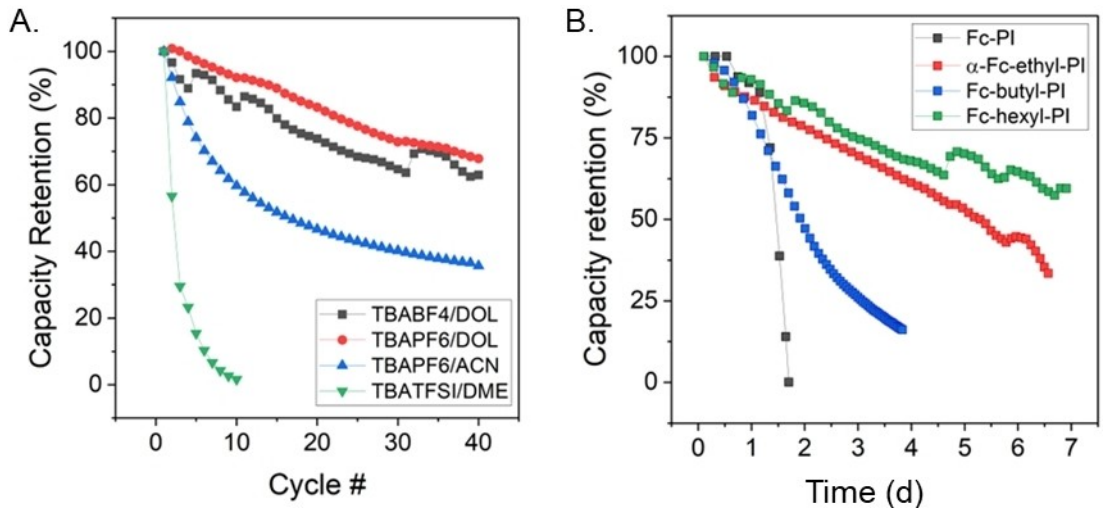

Figure 6. Capacity retention of A) Fc-hexyl-PI in various supporting electrolytes and B) various studied BRMs in 1 6M $TBABF_4$/DOL supporting electrolyte, showing 50 cycles (10 cycles for Fc-PI).

Table 1. Literature BRM performance in NARFBs.

BRM [Pos/Neg]	Capacity [mAh L^{-1}]	Current density [mA cm^{-2}]	Conc. [mM]	Cell potential [V]	Membrane/Separator	Ref.
Nitronyl/Nitroxide	300	1	100	1.62	Fumasep-FAP	[29]
Fc/Anthroquinone	300	2	10	1.42	Daramic AA-250	[30]
TEMPO/Phenazine	313	1	10	1.20	Anion Exchange Membrane	[31]
Phenothiazine/PI	560	10	25	2.31	Daramic A175	[16]
QPT-OMe	600	10	25	2.55	Daramic-175	[32]
Fc-hexyl-PI	1,280	1	50	1.93	Nafion 117	This work

3. Conclusions

Six Fc-*n*-PI BRM derivatives, which have never been tested in flowing cells, were synthesized with various length, polarity, and shielding ability of the linker group. Cumulative charge discharge cycling results of the BRMs reveals that there exists a minimum spacer length to achieve adequate cycling stability and limit membranal diffusion. Additionally, increasing the spacer length (up to hexyl length) does not pose any adverse effect on charge balance or diffusion kinetics of the Fc-*n*-PI derivatives. While steric shielding can dramatically enhance stability and performance of a relatively short spacer, the longest spacer length of six carbons obtained the greatest cycling stability. Fc-hexyl-PI displayed exceptional capacity (1.28 mAh L^{-1}) and cell voltage (1.93 V) compared to other reported BRMs. This cell also exhibited $>98\%$ CE over 100 cycles, owing to the reduced crossover Fc-hexyl-PI due to its bulky and bipolar nature. This work provides valuable insight on the effect of structural modification of BRMs and resultant flow battery performance. Additional studies are needed to understand membrane fouling by radicals and methods to enhance their compatibility in non-aqueous systems.

Experimental Section

Chemicals

$TBABF_4$, $TBAPF_6$, TBATFSI, DOL, MeCN, DME, tetrabutylammonium hydroxide (TBAOH) solution (1 M in methanol) were purchased from Sigma. All chemicals used in synthesis were used as received unless noted otherwise in the procedure (Supporting Information).

Characterization

Proton NMR spectra were obtained at an operating frequency of 500 MHz. Chemical shifts are reported in ppm with the solvent indicated as the internal reference. Coupling constants (*J*) are reported in Hz and the splitting abbreviations used are: s, singlet; d, doublet; t, triplet; q, quartet; m, multiplet; br, broad. Volatile solvents were removed under reduced pressure using a Büchi rotary evaporator and is referred to as removing solvents *in vacuo*. Melting points are reported as the onset and endset points of the melting point endotherm using Differential scanning calorimetry (DSC). DSC was performed at 10 °C min^{-1} under N_2 using 4 to 10 mg of sample. Solubility of BRMs was determined via shake-flask method whereby 1 M $TBABF_4$ in DOL was dropwise added to 0.2 g of BRM until a saturated solution was obtained as determined by visual inspection. FT-IR Spectroscopy was utilized to characterize membranes and electrolyte before and after flow cell cycling. UV-visible spectrophotometer was used to determine BRM concentration in diffusion tests.

Cyclic Voltammetry

Redox behavior of BRMs was investigated via CV using a typical 3-electrode setup. Glassy carbon (0.196 cm^2) was used as the working electrode, Pt wire was used as the counter electrode, and a polished Ag wire electrode filled with working electrolyte was used as a pseudo-reference electrode with ferrocene as an internal reference. Supporting electrolyte of 1 M $TBABF_4$ in DOL was used for CV measurements. Voltammograms were collected prior to flow battery testing at scan rates of 10, 50, 100, and 250 $mV\,s^{-1}$. All electrochemical experiments were conducted in an inert Argon-filled glovebox where oxygen and water concentrations were <1 ppm. Post-mortem voltammograms were recorded at 100 $mV\,s^{-1}$ scan rate. Diffusion constants (D) were calculated from the Randles–Ševčík equation (Eq. (1)).

$$i_p = (2.152 \times 10^5) A C D^{1/2} v^{1/2} \quad (1)$$

where A is electrode area, C is concentration, and v is scan rate. Rate constants (k^0) were determined using Nicholson method via Eq. (2).

$$\varphi = \frac{k^0}{(DnF\pi/RT)^{1/2}} \frac{1}{v^{1/2}} \quad (2)$$

where φ is the Nicholson dimensionless parameter.

Flow Cell Testing

Flow cell performance of the BRMs was analyzed using a laboratory scale 5 cm^2 flow cell (Figure S14 and S15) in an Argon-filled glovebox. Cell end plates, current collector, and graphite serpentine flow fields were purchased from Fuel Cell Technologies. A PTFE gasket with 5 cm^2 opening was cut and used to house the carbon felt electrode (SGL carbon, 2.5 mm thickness, GFD grade). Nafion 117 membrane was pre-treated with TBAOH (1 M in methanol, 24 h), rinsed with DI water, vacuum oven dried (70 °C, 24 h), then finally soaked with electrolyte for 48 h prior to cell assembly. Pretreatment is necessary to avoid proton activated polymerization of DOL solvent (Figure S16). Peristaltic pumps with a flow rate of 20 $mL\,min^{-1}$ were used to flow 10 mL of BRM solution on both sides of the cell. Electrolyte concentration for both posolyte and negolyte were 0.05 M BRM in 1 M $TBABF_4$ in DOL unless otherwise stated. Norprene tubing was used to flow electrolyte through the cell and PTFE tubing was used as the return tube. Electrochemical impedance spectra (EIS) were collected using a potentiostatic 5 mV perturbation over a frequency range of 1 MHz to 1 kHz. Cells were cycled galvanically at a current density of 1 $mA\,cm^{-2}$ at a voltage cutoff range of 1.4 to 2.4 V unless otherwise stated. Post-mortem examination and FT-IR of Nafion membranes were conducted after rinsing the cell with methanol and acetone.

Supporting Information

Supporting Information is available free of charge from https://doi.org/10.1002/celc.202400450.

Conflict of Interests

The authors declare no conflict of interest.

Data Availability Statement

The data that supports the findings of this study are available in the supplementary material of this article. This material is based upon work supported by the U.S. Department of Energy, Office of Electricity (OE), Energy Storage Division. This article has been authored by an employee of National Technology & Engineering Solutions of Sandia, LLC under Contract No. DE-NA0003525 with the U.S. Department of Energy (DOE). The employee owns all right, title and interest in and to the article and is solely responsible for its contents. The United States Government retains and the publisher, by accepting the article for publication, acknowledges that the United States Government retains a non-exclusive, paid-up, irrevocable, world-wide license to publish or reproduce the published form of this article or allow others to do so, for United States Government purposes. The DOE will provide public access to these results of federally sponsored research in accordance with the DOE Public Access Plan https://www.energy.gov/downloads/doe-public-access-plan. This paper describes objective technical results and analysis. Any subjective views or opinions that might be expressed in the paper do not necessarily represent the views of the U.S. Department of Energy or the United States Government.

Keywords: Flow battery · Non-aqueous · Bipolar redox molecule

[1] J. Luo, B. Hu, M. Hu, Y. Zhao, T. L. Liu, *ACS Energy Lett.* **2019**, *4*, 2220–2240. https://doi.org/10.1021/acsenergylett.9b01332.
[2] R. Guchhait, B. Sarkar, *Energies* **2023**, *16*, 2665. https://doi.org/10.3390/en16062665.
[3] A. Weber, M. Mench, J. Meyers, P. Ross, J. Gostick, Q. Liu, *J. Appl. Electrochem.* **2011**, *41*, 1137–1164. https://doi.org/10.1007/s10800-011-0348-2.
[4] Z. Yang, L. Tong, D. P. Tabor, E. S. Beh, M. A. Goulet, D. De Porcellinis, A. Aspuru-Guzik, R. G. Gordon, M. J. Aziz, *Adv. Energy Mater.* **2017**, *8*. https://doi.org/10.1002/aenm.201702056.
[5] P. Leung, A. A. Shah, L. Sanz, C. Flox, J. R. Morante, Q. Xu, M. R. Mohamed, C. Ponce de León, F. C. Walsh, *J. Power Sources* **2017**, *360*, 243–283. https://doi.org/10.1016/j.jpowsour.2017.05.057.
[6] J. Noack, N. Roznyatovskaya, T. Herr, P. Fischer, *Angew. Chem. Int. Ed.* **2015**, *54*, 9776–9809. https://doi.org/10.1002/anie.201410823.
[7] G. Kear, A. A. Shah, F. C. Walsh, *Int. J. Energy Res.* **2012**, *36*, 1105–1120. https://doi.org/10.1002/er.1863.
[8] J. Yuan, C. Zhang, Y. Zhen, Y. Zhao, Y. Li, *J. Power Sources* **2019**, *443*, 227283. https://doi.org/10.1016/j.jpowsour.2019.227283.
[9] C. X. Cammack, H. D. Pratt 3rd, L. J. Small, T. M. Anderson, *Dalton Trans* **2021**, *50*, 858–868. https://doi.org/10.1039/d0dt03927f.
[10] X. Wang, A. Lashgari, J. Chai, J. J. Jiang, *Energy Storage Mater.* **2022**, *45*, 1100–1108. https://doi.org/10.1016/j.ensm.2021.11.008.
[11] M. Li, J. Case, S. D. Minteer, *ChemElectroChem* **2021**, *8*, 1215–1232. https://doi.org/10.1002/celc.202001584.
[12] M. V. Makarova, A. V. Akkuratov, M. E. Sideltsev, K. J. Stevenson, E. I. Romadina, *ChemElectroChem* **2022**, *9*, e202200483.
[13] L. Tang, P. Leung, Q. Xu, C. Flox, *ChemElectroChem* **2024**, *11*, e202400024.
[14] H.-G. Kwon, I. Bae, S.-H. Choi, *J. Membr. Sci.* **2021**, *620*. https://doi.org/10.1016/j.memsci.2020.118928.
[15] R. Wang, M. Li, Y. Liu, G. Dai, T. Wu, W. He, S. Feng, X. Zhang, Y. Zhao, *Electrochem. Commun.* **2023**, *151*, 107509. https://doi.org/10.1016/j.elecom.2023.107509.
[16] J. S. Tracy, E. S. Horst, V. A. Roytman, F. D. Toste, *Chem. Sci.* **2022**, *13*, 10806–10814. https://doi.org/10.1039/D2SC03450F.

[17] M. Li, G. Agarwal, I. A. Shkrob, R. T. VanderLinden, J. Case, M. Prater, Z. Rhodes, R. S. Assary, S. D. Minteer, *J. Mater. Chem. A* **2021**, *9*, 23563–23573. https://doi.org/10.1039/D1TA04821J.
[18] D. Xu, C. Zhang, Y. Zhen, Y. Li, *ACS Appl. Energy Mater.* **2021**, *4*, 8045–8051. https://doi.org/10.1021/acsaem.1c01362.
[19] N. M. Chola, R. K. Nagarale, *New J. Chem.* **2022**, *46*, 22593–22601. https://doi.org/10.1039/D2NJ03495F.
[20] C. Zhang, Z. Niu, Y. Ding, L. Zhang, Y. Zhou, X. Guo, X. Zhang, Y. Zhao, G. Yu, *Chem* **2018**, *4*, 2814–2825. https://doi.org/10.1016/j.chempr.2018.08.024.
[21] G. Yang, Y. Zhai, J. Yao, S. Song, L. Lin, W. Tang, Z. Wen, N. Hu, L. Lu, *Chem. Commun.* **2021**, *57*, 7934–7937. https://doi.org/10.1039/D1CC02916A.
[22] S. Hwang, H.-s. Kim, J. H. Ryu, S. M. Oh, *J. Power Sources* **2018**, *395*, 60–65. https://doi.org/10.1016/j.jpowsour.2018.05.053.
[23] S. Hwang, H.-S. Kim, J. H. Ryu, S. M. Oh, *J. Power Sources* **2019**, *421*, 1–5. https://doi.org/10.1016/j.jpowsour.2019.02.080.
[24] E. M. Fell, M. J. Aziz, *J. Electrochem. Soc.* **2023**, *170*, 100507. https://doi.org/10.1149/1945–7111/acfcde.
[25] K. P. Smith, R. Rungta, A. A. Wang, C. W. Monroe, *J. Electrochem. Soc.* **2023**, *170*, 060510. https://doi.org/10.1149/1945–7111/acd873.
[26] P. P. Sharma, D. Kim, *Membranes (Basel)* **2022**, *12*, 521. https://doi.org/10.3390/membranes12050521.
[27] M. Gao, M. Salla, F. Zhang, Y. Zhi, Q. Wang, *J. Power Sources* **2022**, *527*, 231180. https://doi.org/10.1016/j.jpowsour.2022.231180.
[28] X. Wei, W. Xu, J. Huang, L. Zhang, E. Walter, C. Lawrence, M. Vijayakumar, W. A. Henderson, T. Liu, L. Cosimbescu, B. Li, V. Sprenkle, W. Wang, *Angew Chem Int Ed Engl* **2015**, *54*, 8684–8687. https://doi.org/10.1002/anie.201501443.
[29] T. Hagemann, J. Winsberg, B. Häupler, T. Janoschka, J. J. Gruber, A. Wild, U. S. Schubert, *NPG Asia Mater.* **2017**, *9*, e340. https://doi.org/10.1038/am.2016.195.
[30] Y. Zhen, C. Zhang, J. Yuan, Y. Zhao, Y. Li, *J. Power Sources* **2020**, *480*, 229132. https://doi.org/10.1016/j.jpowsour.2020.229132.
[31] J. Winsberg, C. Stolze, S. Muench, F. Liedl, M. D. Hager, U. S. Schubert, *ACS Energy Lett.* **2016**, *1*, 976–980. https://doi.org/10.1021/acsenergylett.6b00413.
[32] Y. Li, G. Dai, Y. Chen, R. Wang, H. Li, X. Shi, X. Zhang, Y. Xu, Y. Zhao, *ACS Energy Lett.* **2022**, *7*, 1274–1283. https://doi.org/10.1021/acsenergylett.2c00198.

Manuscript received: July 23, 2024
Revised manuscript received: August 20, 2024
Version of record online: ■■, ■■

RESEARCH ARTICLE

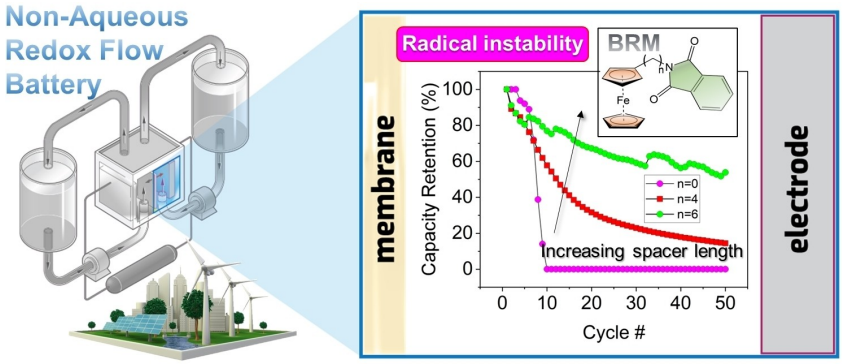

S. Macchi, C. L. Staiger, J. Cordova, C. Poirier, T. M. Anderson*

A series of ferrocene-phthalimide bipolar redox molecules with varying linkers are synthesized for non-aqueous flow batteries. Cycling stability of the flow batteries is greatly improved via physical separation or steric shielding.